Imaging of integer quantum Hall edge state in a quantum point contact via scanning gate microscopy

N. Aoki,[1,2] C. R. da Cunha,[1] R. Akis,[1] D. K. Ferry,[1] and Y. Ochiai[2]
[1]*Department of Electrical Engineering and Center for Solid State Electronics Research, Arizona State University, Tempe, AZ 85287-5706, USA*
[2]*Department of Electronics and Mechanical Engineering, Chiba University, 1-33 Yayoi-cho, Inage-ku, Chiba 263-8522, Japan*
(Received 26 April 2005; revised manuscript received 25 July 2005; published 26 October 2005)

Integer quantum Hall edge states have been imaged in the constriction region of a quantum point contact fabricated in an InGaAs heterostructure at high magnetic fields using low-temperature scanning gate microscopy (SGM). Features in the SGM images grew wider and deeper as side gates squeezed the constriction. Furthermore, clear plateaus corresponding to the depopulation of edge states were observed. We propose a model for these images based on the variation of the local confinement potential induced by the tip.

DOI: 10.1103/PhysRevB.72.155327 PACS number(s): 73.43.−f, 68.65.−k, 07.79.Lh

The quantum Hall (QH) effect is one of the unique phenomena that appear in a high-mobility two-dimensional electron gas (2DEG) at high magnetic fields, and has been widely investigated since its discovery.[1,2] The transport regime is well understood by the current carried by edge channels propagating along the edges of the sample,[3–6] and many experiments have been performed to directly visualize the evidence of this feature in the QH regime. In the early stages of investigation of this regime, transport measurements using the top gate technique have been performed for selecting edge channels.[7,8] Later, local probing methods such as optical techniques,[9,10] inductive probing,[11] single electron transistor probing,[12] and even scanning gate measurements[13] have followed. However, the spatial resolution obtained with these techniques is typically limited to several microns. In order to detect fine local information, attention has recently been paid to scanning probe microscopy techniques. For instance, a single-electron transistor fabricated on the end of a tip has been used to detect local charges on the regions corresponding to edge channels,[14] an induced few-electron bubble has been used at high frequencies to detect charges entering and leaving this region,[15] and other techniques such scanning potential microscopy[16] and Kelvin force microscopy[17] have also been used to detect the local force gradient produced by the QH effect.

Scanning gate microscopy (SGM) is a tool that has been used to detect many transport characteristics of quantum structures. For instance, electron flow images through a quantum point contact (QPC) have been obtained by disturbing current paths by a tip-induced potential.[18] Moreover, single electron manipulation has been demonstrated by scanning a biased tip on a quantum dot in the Coulomb blockade regime.[19] In most of these techniques, SGM works by perturbing the transmission through the device and measuring a corresponding change in conductance. However, in the QH regime, the transverse conductance is quantized, whereas the longitudinal resistance is near zero, which makes it extremely difficult to visualize the edge states by conductance variations at large scales. The edge states are pushed close together within a QPC. Thus, the biased tip can enhance scattering between edge states, and induce backscattering that has a direct effect in the measured conductance. This has the potential of providing a simple measurement of the nature of compressible and incompressible edge states.[20] In this paper, we use in-plane gates to form a QPC in which we are able to perform SGM within the QPC.

The sample was fabricated in an InAlAs/InGaAs/InAlAs heterostructure whose modulation-doping layer is situated above the quantum well. The latter is located 45 nm below surface. Shubunikov-de Haas (SdH) measurement [Fig. 1(a)] shows that the 2DEG has two subbands occupied, and their carrier densities are 7.2×10^{11} cm^{-2} and 2.1×10^{11} cm^{-2}, respectively. The occupation of two subbands, nevertheless, does not seem to change the nature of the experiment. The total mobility obtained from the total carrier density is 7.4×10^{4} cm^{-2}/V s, and the corresponding mean free path is 1.2 μm. The QPC was defined with etched trenches as shown in the inset of Fig. 1(a). The radius of curvature at the top of the outer edges of the QPC is 0.8 μm and the separation that defines the constriction is approximately 0.6 μm. This structure allows us to use the 2DEG inside the trenches as side gates by biasing the in-plane materials. The trenches are approximately 20 nm deeper than the bottom of the quantum well, which ensures a complete electrical isolation for the in-plane gates up to −10 V. Often, when locating a device by taking images of the topography in contact mode, electrical leakage from the tip to the surface can occur, destroying the device. In order to prevent such accidents, the sample was coated with 25 nm of polymethylmethacrylate (PMMA).

For the SGM measurements, a low-temperature scanning probe microscopy head was installed in a He^3 cryostat. The system has a scanning area of 2.7×2.7 μm^2 at 300 mK and holds this base temperature for more than 40 h with the pumps off. In order to avoid heating and carrier generation from a conventional laser detection system, a piezoresistive cantilever was used. This tip was coated with 15 nm of $PtIr_{20}$. Although, contact mode was used for taking topographical images, lift mode was used to perform SGM measurements. In this configuration, the tip is lifted 45 nm above the surface in order to achieve suitable levels of perturbation. During SGM imaging, the tip bias (V_{tip}) is kept at −1 V, and

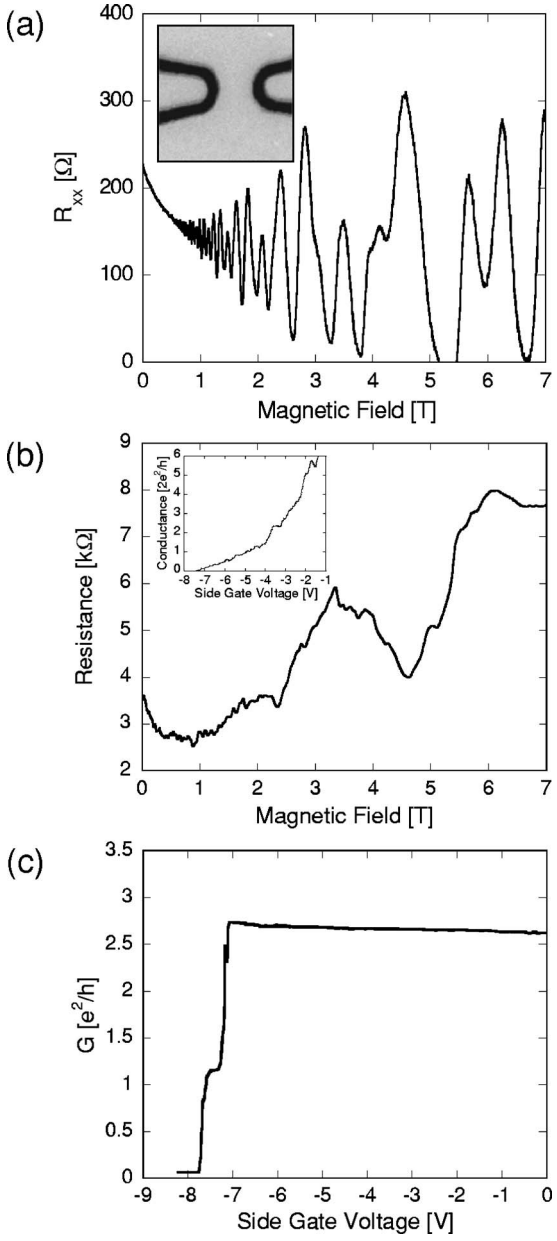

FIG. 1. (a) Shubinikov de Haas oscillations of the 2DEG at 0.3 K. The inset shows the topographical image of the QPC defined by etched trenches. The scanning area is $2.7\times2.7\ \mu m^2$. (b) Magnetoresistance of the QPC at $V_g=-2.5$ V. The inset shows the transmission curve of the QPC at zero magnetic field. (c) Transmission curve of the QPC at 6.6 T.

the gate bias voltage (V_g) varies between 0 and −7.5 V depending on the measurement. The tip bias and lift height play an important role as they define the shape and strength of the perturbation. As the tip is pulled away from the surface, the distribution of its electric field widens at the 2DEG region, producing a wider and smoother depletion region. Furthermore, the difference between the work function of the tip and the electron affinity of the material is enough to generate a depletion region. Therefore, small tip biases are enough to cause some level of scattering. In our case, it was found that −1 V is enough to overcome the signal-to-noise ratio. The voltage drop across the device and the current that flows through it are measured simultaneously using two lock-in amplifiers in a four-probe configuration. Quasiconstant current excitation (typically 10 nA) is used at a frequency of 1.7 kHz and an integration time of 30 ms in order to achieve an acceptable bandwidth for the measurements. The data is stored in a computer synchronized with the tip position to obtain a map of the conductance across the sample.

The magnetoresistance measured across the QPC at $V_g=-2.5$ V is shown in Fig. 1(b). At low magnetic fields, the curve displays many fluctuations because of quantum interference.[21] This also affects the transmission curve as shown in inset of Fig. 1(b). At high magnetic fields, however, the geometrical barrier is suppressed and the transport enters the QH regime. This magnetotransmission curve differs from SdH measurements in the sense that the quantum constriction depopulates subbands, making its analysis more complicated. Nonetheless, the transmission curve displays a clear change in behavior at 6.6 T, as shown in Fig. 1(c). Two clear steps are observed at 2.8 and 1.2 G_0 ($G_0=e^2/h$), which indicates that two edge states are propagating through the QPC at $V_g=0$ V (a shunt resistance has not been removed). These depopulate to one edge state at $V_g=-7.0$ V and pinch off at −7.7 V. According to the carrier density of the 2DEG, the filling factors for the first and the second subbands in the bulk are approximately 5 (4.8 calculated) and 1 (1.2 calculated) at 6.6 T, respectively. However, no signature of transmission of the second subband is observed in the QPC, which indicates that the edge state corresponding to the second subband is completely reflected by the constriction. Considering that four out of five edge channels are reflected by the constriction, the conductance can be estimated as 1.3 G_0 using

$$G = G_0 \frac{N(N-K)}{K},$$

where N is the number of edge channels in 2DEG, and K is the number of reflected edge channels.[8] Using the same argument, a conductance of 3.4 G_0 is found for the second plateau. One of the reasons for the small difference between the estimated and measured conductance values is the partial filling of Landau levels in the 2DEG.

Two-dimensional maps of SGM images are shown in Figs. 2(a)–2(e) for several side-gate voltages. Keeping $V_{tip}=-1$ V and the tip-to-surface gap 45 nm, no change in the SGM images was observed between $V_g=0$ and −3.4 V. Changes in conductance start to appear from −3.8 V. Measurements where the tip bias was increased to −2.5 V reveal that this onset was moved to −0.8 V. From this, one infers that the size of the depletion region changes approximately three times more with the tip bias than with the in-plane gates for this tip-to-2DEG gap. The images at $V_{tip}=-1$ V begin to display features that grow wider and deeper. In Figs. 2(a)–2(d), the base conductance far from the constriction takes a constant value of about 2.8 G_0, which corresponds to the conductance of the second plateau in Fig. 1(c). Moreover, a flat region was observed at around 1.2 G_0 in the images that correspond to the first plateau in Fig. 1(c). Figure 2(f) shows line profiles at the center of the constriction with dif-

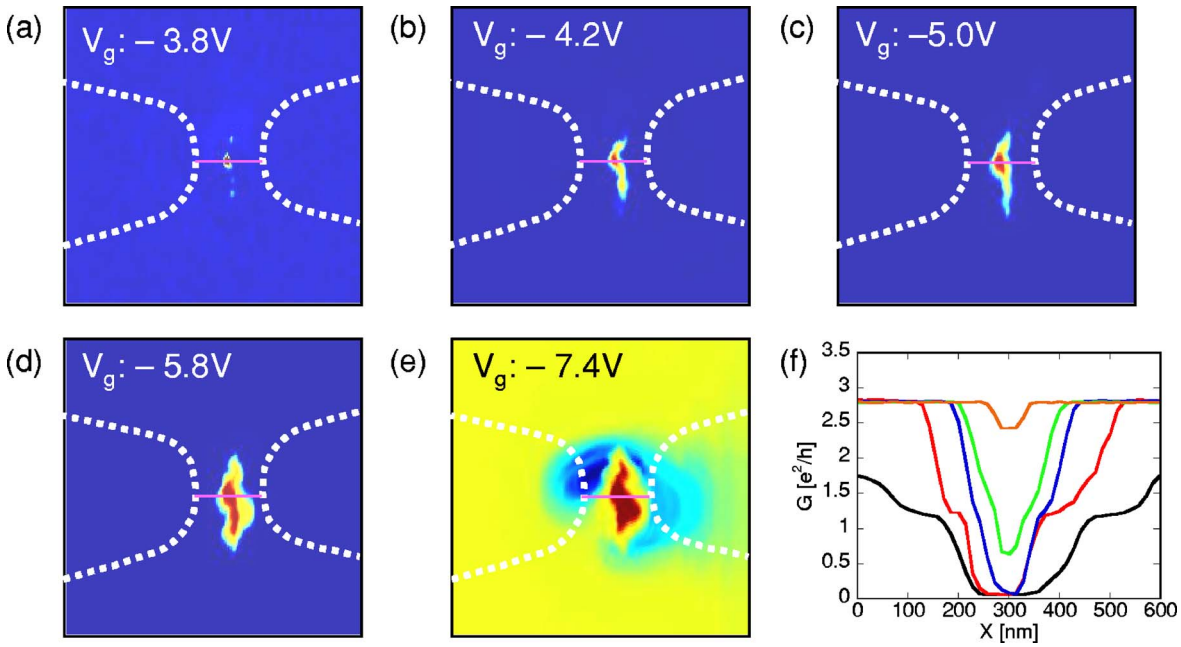

FIG. 2. (Color online) Two-dimensional plots of the images of conductance variation at 6.6 T at various side-gate voltages; (a) −3.8 V, (b) −4.2 V, (c) −5 V, (d) −5.8 V, (e) −7.4 V. The scanning area is 2.7×2.7 μm^2. The dotted lines indicate the outer edge of the trenches. (f) Line profiles obtained at the center region of the QPC. A red line in the images indicates where the line profiles were taken. The curves, from the inner to the outer, correspond to the profiles of images (a) to (e).

ferent gate voltages to illustrate these values of conductance. Increasing the negative gate voltage, the base conductance drops in a way similar to the transmission curve. Figure 2(e) was taken at the transition point between the first and the second plateaus. When the base conductance is at the first plateau, it is only possible to see a transition to a condition of total pinchoff in Fig. 2(f).

For further analysis of the images, a two-dimensional image and the corresponding three-dimensional plot at V_g= −5.4 V are shown in Fig. 3(a) and 3(b), respectively. The shape of the region where the conductance is varying is somewhat curious and asymmetric, and unlike previous measurements at low magnetic field, does not exhibit quantum interference patterns.[21] To understand the shape of the images, one has to consider that the effect of the tip potential is to induce a depletion region in the 2DEG region. Far from the constriction, the effect of the tip is negligible, as it does not have the capability of depopulating edge states. However, when the tip moves near the constriction, the tip-induced depletion makes the edge states flow along its potential. As the tip moves more towards the center, it eventually causes the two innermost stripes to touch each other and backscatter, causing a depopulation of these edge states. Thus, the role of the tip potential is to compress the edge states towards each other by lifting the local potential. This is very similar to the change in conductance with increasing side-gate voltage; however, our SGM results show the spatial distribution of the integer edge states in the constriction. Clear plateaus can be observed at around 1.2 G_0 at both sides in Fig. 3(b). There are two compressible edge states in the constriction, and the tip is assumed to move from the right side to the center of the constriction along the solid line in Fig. 3(b). If the tip is far from the constriction, the induced potential is not strong enough to backscatter the inner compressible edge channels, and consequently the conductance is maintained (region *i*). When the innermost compressible edge channels start to interact and backscatter, the conductance begins to decrease (region *ii*). From this, it is possible to obtain an estimate for the width of the compressible region. For instance, the first decay on region *ii* has a width of approximately 60 to ~130 nm, which corresponds to the onset and complete of intersection of the two innermost compressible regions. Thus, each compressible stripe has an approximate width of 30–65 nm. Until the next compressible stripe starts to backscatter, the conductance is main-

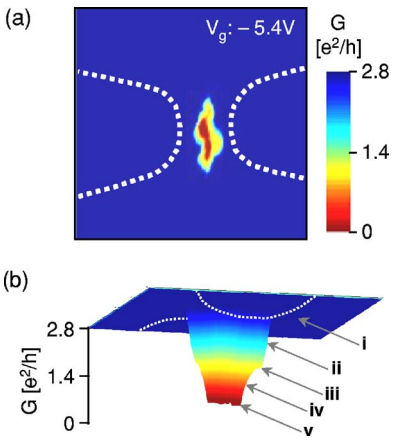

FIG. 3. (Color online) (a) Two-dimensional SGM image at V_g =−5.4 V. The dotted lines indicate the outer edge of the trenches. (b) The corresponding three-dimensional plot of the image. The indications (*i*–*v*) are corresponding to the characteristic regions in the image.

tained (region *iii*). Squeezing the constriction further, the last compressible regions begin to merge (region *iv*), and finally the constriction is pinched off (region *v*). From this scenario, it is also possible to obtain the width of the incompressible stripe, which is approximately 15–20 nm. This matches the description shown in Ref. 20 of incompressible stripes being narrower than the compressible ones. Considering the fact that the shape of the images are similar even for different gate voltages, it strongly suggests that the shape of the images is highly influenced by static features such as the roughness of the potential wall formed by the side gates and the background disordered potential. Such features have also been visualized by SGM when the conductance is brought near the pinchoff point at zero magnetic field.[21]

No evidence of a fractional edge channel was observed in this experiment probably because of the low mobility of this material. This, perhaps, would be possible to observe if the QPC were fabricated on a high-mobility sample such as GaAs/AlGaAs heterostructure.[22] Furthermore, one expects the in-plane materials to also enter the QH regime. Although the electrostatic potential caused by the gates is unchanged, this might change screening effects in the channel, which changes the widths of the compressible stripes according to the description given in Ref. 20. This effect may produce measurements that diverge from the real widths of the compressible stripes. Another point of relevance is the increase in conductance in the regions corresponding to the in-plane gates, as observed in Fig. 2(e). This is likely caused by the tip-induced potential pushing edge states in the in-plane gates away from the physical edge, which, in turn, increases the effect width of the channel.

In summary, we have studied transport in the QH regime in the constriction of a QPC via low-temperature SGM. A spatial distribution of the integer edge states has been visualized as images of conductance variation. In these images, clear plateaus have been observed at the same conductance values of the transmission curve. These images are understood as the tip-induced potential locally depopulates the edge channels propagating through the QPC. With the technique, estimations for the widths of compressible and incompressible stripes are obtained, and have a ratio similar to that proposed in previous theoretical works. Interesting as well is the fact that the measurement is, to some extent, independent of the size of the depletion region, as its function is to push the edge states towards each other.

The authors would like to thank Andre Beyer and Razib Shishir for help with sample preparation, and S. M. Goodnick, and J. Smöliner for many helpful discussions, as well as for the hospitality of the group at the Technical University of Vienna during visits of C. R. Da Cunha. This work was supported by the Office of Naval Research.

[1] K. v. Klitzing, G. Dorda, and M. Pepper, Phys. Rev. Lett. **45**, 494 (1980).
[2] B. J. van Wees, L. P. Kouwenhoven, E. M. M. Willems, C. J. P. M. Harmans, J. E. Mooij, H. van Houten, C. W. J. Beenakker, J. G. Williamson, and C. T. Foxon, Phys. Rev. B **43**, 12431 (1991).
[3] M. Büttiker, Phys. Rev. B **38**, 9375 (1988).
[4] B. I. Halperin, Phys. Rev. B **25**, 2185 (1982).
[5] C. W. J. Beenakker, Phys. Rev. Lett. **64**, 216 (1990).
[6] A. M. Chang, Solid State Commun. **74**, 871 (1990).
[7] R. J. Haug, A. H. MacDonald, P. Streda, and K. von Klitzing, Phys. Rev. Lett. **61**, 2797 (1988).
[8] J. M. Ryan, N. F. Deutscher, and D. K. Ferry, Phys. Rev. B **48**, 8840 (1993).
[9] A. A. Shashkin, A. J. Kent, P. A. Harrison, L. Eaves, and M. Henini, Phys. Rev. B **49**, 5379 (1994).
[10] R. J. F. van Haren, F. A. P. Blom, and J. H. Wolter, Phys. Rev. Lett. **74**, 1198 (1995).
[11] E. Yahel, A. Tsukernik, A. Palevski, and H. Shtrikman, Phys. Rev. Lett. **81**, 5201 (1998).
[12] Y. Y. Wei, J. Weis, K. v. Klitzing, and K. Eberl, Phys. Rev. Lett. **81**, 1674 (1998).
[13] S. Kicin, A. Pioda, T. Ihn, K. Ensslin, D. C. Driscoll, and A. C. Gossard, Phys. Rev. B **70**, 205302 (2004).
[14] A. Yacoby, H. Hess, T. Fulton, L. P. Pfeiffer, and K. West, Solid State Commun. **1**, 111 (1999).
[15] G. Finkelstein, P. Glicofridis, R. Ashoori, and M. Shayegan, Science **289**, 90 (2000).
[16] K. L. McCormick, M. T. Woodside, M. Huang, M. Wu, P. L. McEuen, C. Duruoz, and J. S. Harris, Phys. Rev. B **59**, 4654 (1999).
[17] P. Weitz, E. Ahlswede, J. Weis, K. von Klitzing, and K. Eberl, Physica E (Amsterdam) **247**, 6 (2000).
[18] M. A. Topinka, B. J. LeRoy, S. E. J. Shaw, E. J. Heller, R. M. Westervelt, K. D. Maranowski, and A. C. Gossard, Science **289**, 2323 (2000); M. A. Topinka, B. J. LeRoy, R. M. Westervelt, S. E. J. Shaw, R. Fleischmann, E. J. Heller, K. D. Maranowski, and A. C. Gossard, Nature (London) **410**, 183 (2001); M. A. Topinka, B. J. LeRoy, R. M. Westervelt, K. D. Maranowski, and A. C. Gossard, Physica E (Amsterdam) **12**, 678 (2002); R. Crook, C. G. Smith, M. Y. Simmons, and D. A. Ritchie, J. Phys.: Condens. Matter **12**, L735 (2000).
[19] A. Pioda, S. Kicin, T. Ihn, M. Sigrist, A. Fuhrer, K. Ensslin, A. Weichselbaum, S. E. Ulloa, M. Reinwald, and W. Wegscheider, Phys. Rev. Lett. **93**, 216801 (2004).
[20] D. B. Chklovskii, K. A. Matveev, and B. I. Shklovskii, Phys. Rev. B **47**, 12605 (1993).
[21] C. R. da Cunha, N. Aoki, R. Akis, D. K. Ferry, and Y. Ochiai (unpublished).
[22] M. Ando, A. Endo, S. Katsumoto, and Y. Iye, Solid-State Electron. **42**, 1179 (1998).